Coarsening dynamics of biaxial nematic liquid crystals

N. V. Priezjev and Robert A. Pelcovits
Department of Physics, Brown University, Providence, Rhode Island 02912
(Received 27 June 2002; published 13 November 2002)

We study the coarsening dynamics of two- and three-dimensional biaxial nematic liquid crystals, using Langevin dynamics. Unlike previous work, we use a model with no *a priori* relationship among the three elastic constants associated with director deformations. Biaxial nematics possess four topologically distinct classes of defects, three of which have half-integer charge, while the fourth, which plays a minor role in coarsening, is of integer charge. We find a rich variety of coarsening behavior, including the presence of one, two, or three of the half-integer classes at late times, depending on the relative values of the elastic constants and the resulting energetics of the decay channels of the defects. The morphology of the defect tangle in three dimensions when all three classes are present is particularly interesting. Rather than forming independent defect loops (as occurs when only one or two of the classes are present), the defect lines meet at junction points which are distributed uniformly throughout the system. As the system coarsens some pairs of neighboring junction points approach each other and annihilate, allowing the formation of nonintersecting loops each formed from a single defect class. These loops then shrink independently during the very final stages of the coarsening sequence.

DOI: 10.1103/PhysRevE.66.051705 PACS number(s): 64.70.Md, 61.30.Jf

Topological defects play an important role in the equilibration process following a quench from a disordered to an ordered phase (''coarsening dynamics''). Coarsening dynamics in nematic liquid crystals, particularly with uniaxial ordering, has been the subject of much active investigation in recent years in theory, experiments, and simulations [1–4], in part because of the rich defect structure of liquid crystals. On the other hand, relatively little attention (with the exception of the two-dimensional work of Ref. [2]) has been paid to coarsening dynamics in biaxial liquid crystals, in part because of the dearth of experimental realizations of biaxial liquid crystalline phases. However, biaxial nematics have many unusual topological features, which might be expected to influence their coarsening dynamics and thus warrant study. Biaxial nematics differ from their uniaxial counterparts in that they possess four topologically distinct classes of line defects (disclinations), while possessing no stable point defects (except in two dimensions where the line defects reduce to points) [5,6]. The classes of disclination lines are distinguished by the rotation of the long and short axes of the rectangular building blocks of the system. In the first three classes one of the three axes is uniformly ordered, while the remaining two axes rotate by 180° about the core of the defect. The fourth class consists of 360° rotations of two of the three axes. The disclination lines form closed loops in three dimensions (with a single defect class per loop) or form a network where three lines, each from a different class meet at junction points [7]. The fundamental homotopy group of biaxial nematics is non-Abelian leading to a number of interesting consequences. E.g., the merging of two defects will depend on the path they follow, and two 180° disclinations of different types will be connected by a 360° ''umbilical'' cord after crossing each other [8].

Zapotocky *et al.* [2] studied coarsening dynamics in a two-dimensional model of biaxial nematics, utilizing a cell-dynamical scheme applied to a Landau-Ginzburg model, where the gradient portion of the energy was given by

$$F_{\mathrm{grad}}=\frac{1}{2}M(\partial_\alpha Q_{\beta\gamma})(\partial_\alpha Q_{\beta\gamma}). \tag{1}$$

Here M is a coupling constant, and $Q_{\alpha\beta}$ is the symmetric-traceless nematic order parameter tensor. Repeated indices are summed over; in the case of a two-dimensional nematic, α is summed over x and y, while β and γ are summed over x, y, and z. Zapotocky *et al.* found that of the four topologically distinct classes of disclinations, only two classes (both corresponding to ''half-integer'' defect points, i.e., 180° rotations) were present in large numbers at late times. Subsequently, Kobdaj and Thomas [9] showed within this one-elastic constant approximation that one class of half-integer disclinations is always energetically unstable towards dissociation into disclinations of the other two half-integer classes.

In this paper we show that if one considers a more general gradient energy the coarsening dynamics of biaxial nematics is much richer than what occurs with the above simple model. In particular, with appropriate sets of parameters one can obtain a coarsening sequence with all three classes of half-integer disclinations present in nearly equal numbers even at late times, or a sequence with only one class of half-integer disclinations surviving until late times. When all three classes are present, the topology of the coarsening sequence in three dimensions is markedly different from the uniaxial case.

To understand why the model free energy of Eq. (1) is not general enough for coarsening studies, it is helpful to see what it yields for the director elastic constants. For biaxial nematics there are three directors which form an orthonormal triad of vectors $\mathbf{u},\mathbf{v},\mathbf{w}$ describing the alignment of the constituent ''bricklike'' molecules; we assume that the longest axis of the molecule is parallel to $\mathbf{w}$. The tensor $Q_{\alpha\beta}$ can be written in terms of the orthonormal triad as

$$Q_{\alpha\beta}=S\left(w_\alpha w_\beta-\frac{1}{3}\delta_{\alpha\beta}\right)+T(u_\alpha u_\beta-v_\alpha v_\beta), \tag{2}$$

where S and T are, respectively, the uniaxial and biaxial order parameters, and $S<3T$ [2]. If we insert Eq. (2) into Eq. (1), we find [10]

$$\begin{aligned}F_{\rm grad}=&K_u[(\mathbf{u}\cdot\boldsymbol{\nabla}\mathbf{v}\cdot\mathbf{w})^2+(\mathbf{v}\cdot\boldsymbol{\nabla}\mathbf{v}\cdot\mathbf{w})^2+(\mathbf{w}\cdot\boldsymbol{\nabla}\mathbf{w}\cdot\mathbf{v})^2]\\&+K_v[(\mathbf{v}\cdot\boldsymbol{\nabla}\mathbf{w}\cdot\mathbf{u})^2+(\mathbf{u}\cdot\boldsymbol{\nabla}\mathbf{u}\cdot\mathbf{w})^2+(\mathbf{w}\cdot\boldsymbol{\nabla}\mathbf{w}\cdot\mathbf{u})^2]\\&+K_w[(\mathbf{w}\cdot\boldsymbol{\nabla}\mathbf{u}\cdot\mathbf{v})^2+(\mathbf{u}\cdot\boldsymbol{\nabla}\mathbf{u}\cdot\mathbf{v})^2+(\mathbf{v}\cdot\boldsymbol{\nabla}\mathbf{v}\cdot\mathbf{u})^2],\end{aligned} \tag{3}$$

where

$$\begin{aligned}K_u&=2M(S+T)^2,\\K_v&=2M(S-T)^2,\\K_w&=8MT^2.\end{aligned} \tag{4}$$

Thus, there are three elastic constants K_u, K_v, K_w each corresponding to one of the three classes of line defects. Each class corresponds to rotations of two of the three vector fields $\mathbf{u},\mathbf{v},\mathbf{w}$, about the defect core, with the third vector of the triad undistorted. We denote the classes as follows [6,7]: C_u ($\mathbf{u}$ undistorted), C_w ($\mathbf{w}$ undistorted), and C_v ($\mathbf{v}$ undistorted). The energy of a defect in class C_i, $i=u,v,w$ is proportional to the elastic constant K_i. Note, however, that in the model specified by Eq. (1) only two of the three elastic constants are independent, as they are related as indicated in Eq. (4). In fact, the specific relationship among the three elastic constants gives rise, as shown in Ref. [9], to the presence of only two defect classes at late times. Irrespective of the values of S and T (M simply sets the overall scale of all three elastic constants), one of the three elastic constants is *always* greater than the sum of the other two, yielding a decay channel for the defect in the class with the largest elastic constant.

There is no symmetry reason to restrict our attention to the model free energy, Eq. (1). Even if we neglect the elastic anisotropy associated with bend, splay and twist distortions, a biaxial nematic should be described in general by three *independent* elastic constants, K_u, K_v, and K_w [10]. In terms of the order parameter tensor $Q_{\alpha\beta}$, this requires a term of third order in $F_{\rm grad}$,

$$F_{\rm grad}=\frac{1}{2}M(\partial_\alpha Q_{\beta\gamma})(\partial_\alpha Q_{\beta\gamma})+LQ_{\alpha\beta}(\partial_\rho Q_{\alpha\gamma})(\partial_\rho Q_{\beta\gamma}), \tag{5}$$

which upon substituting Eq. (2) yields the elastic constants:

$$\begin{aligned}K_u&=2[M(S+T)+LST](S+T),\\K_v&=2[M(S-T)-LST](S-T),\\K_w&=4(2M-LT)T^2.\end{aligned} \tag{6}$$

Because of the extra coupling constant L, there is no predetermined hierarchy among these elastic constants. Unlike the model of Eq. (1) it is now possible with appropriate choices of S,T, and the ratio L/M to have all three elastic constants equal (which will give rise as we demonstrate below to a coarsening sequence with nearly equal populations of the three classes of half-integer defects), or have two constants nearly equal with the third significantly smaller, yielding a coarsening sequence with only one class of defects at late times, or recover the behavior seen in Ref. [2].

To simulate the coarsening dynamics of this general model of biaxial nematics, we consider its lattice analog introduced by Straley [11]. In this model the interaction between two biaxial objects located at sites i and j of a cubic lattice with orientations specified by the orthonormal triad $\mathbf{u},\mathbf{v},\mathbf{w}$ is given by

$$\begin{aligned}U_{ij}=&-\frac{3}{2}\beta(\mathbf{w}_i\cdot\mathbf{w}_j)^2-2\gamma[(\mathbf{u}_i\cdot\mathbf{u}_j)^2-(\mathbf{v}_i\cdot\mathbf{v}_j)^2]\\&-\frac{\delta}{2}[(\mathbf{u}_i\cdot\mathbf{u}_j)^2+(\mathbf{v}_i\cdot\mathbf{v}_j)^2-(\mathbf{u}_i\cdot\mathbf{v}_j)^2-(\mathbf{v}_i\cdot\mathbf{u}_j)^2].\end{aligned} \tag{7}$$

This model has a phase diagram with two uniaxial phases, one with rodlike order (alignment of the $\mathbf{w}$ vector field), one with discotic order (alignment of the $\mathbf{u}$ vector field) and a biaxial phase with alignment of all three vector fields [11–13].

The elastic constants emerging from Eq. (7) can be determined by considering the interaction between two objects which are aligned in turn along each of the three directions $\mathbf{u},\mathbf{v},\mathbf{w}$, with the results:

$$\begin{aligned}K_u&=\frac{3\beta}{2}-2\gamma+\frac{\delta}{2},\\K_v&=\frac{3\beta}{2}+2\gamma+\frac{\delta}{2},\\K_w&=2\delta.\end{aligned} \tag{8}$$

As in the continuum model Eq. (3), the parameters β, γ, and δ give rise to three independent elastic constants. Stability requires that $3\beta+\delta>4|\gamma|$, and $\beta,\delta>0$. Note that $\gamma\rightarrow-\gamma$ is equivalent to the interchange: $\mathbf{u}\leftrightarrow\mathbf{v}$.

As discussed in Refs. [2,9], coarsening in a biaxial system can proceed by annihilation via decay channels where a pair of defects from two different classes annihilates to form a defect of the third class. Specifically, we have three such channels here for the half-integer defect classes:

$$C_u+C_v\rightarrow C_w,\quad \alpha \text{ channel} \tag{9}$$

$$C_u+C_w\rightarrow C_v,\quad \beta \text{ channel} \tag{10}$$

$$C_v+C_w\rightarrow C_u,\quad \gamma \text{ channel}, \tag{11}$$

with associated gains in free energy:

$$\Delta K_\alpha\equiv K_u+K_v-K_w=3-\delta, \tag{12}$$

$$\Delta K_\beta\equiv K_u+K_w-K_v=2\delta-4\gamma, \tag{13}$$

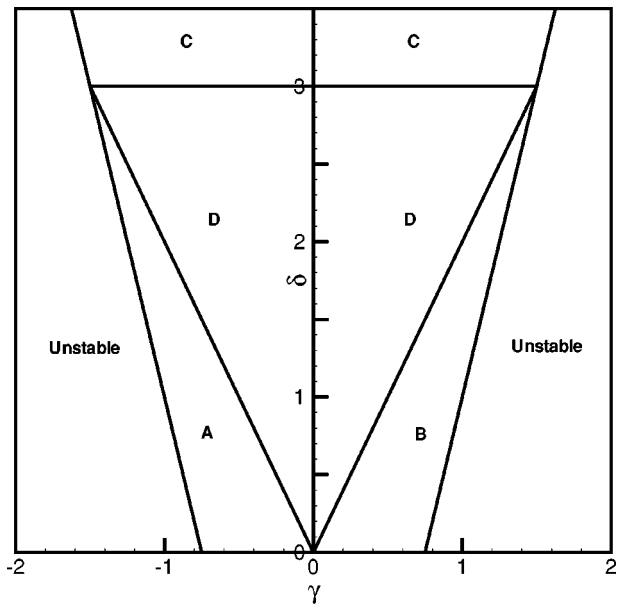

FIG. 1. Parameter space for the model given by Eq. (7), with $\beta=1$. The physically unstable regions on the left and right correspond to $K_v<0$ and $K_u<0$, respectively (i.e., $3\beta+\delta<4|\gamma|$). The boundary between regions *A* and *D* is the line $\delta=-2\gamma$, and the boundary between regions *B* and *D* is the line $\delta=2\gamma$. The boundaries of regions *A*–*D* are determined by the signs of the free energy differences $\Delta K_\alpha, \Delta K_\beta, \Delta K_\gamma$, as explained in the text.

$$\Delta K_\gamma \equiv K_v + K_w - K_u = 2\delta + 4\gamma, \tag{14}$$

respectively.

Fig. 1 shows the parameter space (γ, δ) for the model Eq. (7) with $\beta=1$. The space can be divided into nonoverlapping regions on the basis of the signs of $\Delta K_\alpha, \Delta K_\beta$, and ΔK_γ. Based on these signs we expect the following behavior:

Region *A*. $\Delta K_\alpha, \Delta K_\beta > 0$, $\Delta K_\gamma < 0$. Thus, the decay channels $C_u + C_v \rightarrow C_w$ and $C_u + C_w \rightarrow C_v$ are energetically favorable while $C_v + C_w \rightarrow C_u$ is not; defects of class C_u should *not* be present at late times.

Region *B*. $\Delta K_\alpha, \Delta K_\gamma > 0$, $\Delta K_\beta < 0$. Decay channels $C_u + C_v \rightarrow C_w$ and $C_v + C_w \rightarrow C_u$ are energetically favorable while $C_u + C_w \rightarrow C_v$ is not; defects of class C_v should *not* be present at late times.

Region *C*. ΔK_β, $\Delta K_\gamma > 0, \Delta K_\alpha < 0$. Decay channels $C_u + C_w \rightarrow C_v$ and $C_v + C_w \rightarrow C_u$ are energetically favorable while $C_u + C_v \rightarrow C_w$ is not; defects of class C_w should *not* be present at late times.

Region *D*. $\Delta K_\alpha, \Delta K_\beta, \Delta K_\gamma > 0$. All three decay channels are now favorable, but to varying degrees, depending on values of γ and δ. Near each of the vertices of the triangular region *D*, two of the three channels involve free energy gains that are very small. The remaining channel which corresponds to a large free energy gain will dominate, and we expect a coarsening sequence with only *one* class of defects at late times. This class will be C_w near the origin $\gamma=\delta=0$; C_u near the vertex where regions *B*, *C*, and *D* meet, and C_v near the remaining vertex where regions *A*, *C*, and *D* meet. At the point $\gamma=0$, $\delta=1$, the three elastic constants K_u, K_v, and K_w are equal, and all three decay channels are equally favorable. Thus, at this point (and in its immediate neighborhood) we expect to see all three defect classes represented at late times in the coarsening sequence. Elsewhere in region *D*, two of the three decay channels will be favorable, leading to the survival of the corresponding defect classes at late times.

While these simple free energy arguments suggest what the relative populations of the defect classes will be at different points in the parameter space of our model, they cannot determine what the morphology of the defect tangle in three dimensions will be. If two defect classes are present at late times, are the loops entangled? If three defect classes are present, do they form loops, each of a single defect class, or a network of junction points where three defect lines, one from each class meet?

To answer these questions (and verify that our free energy arguments correctly describe the relative defect populations), we have simulated the coarsening dynamics associated with the model Eq. (7) using Langevin dynamics, expressing the three unit vectors **w**, **u**, and **v** in terms of Euler angles ϕ, θ, and ψ. The equations of motion are given by

$$\zeta \frac{\partial \phi_i}{\partial t} = -\frac{\partial U}{\partial \phi_i} + R_\phi(t),$$

$$\zeta \frac{\partial \cos\theta_i}{\partial t} = -\frac{\partial U}{\partial \cos\theta_i} + R_\theta(t),$$

$$\zeta \frac{\partial \psi_i}{\partial t} = -\frac{\partial U}{\partial \psi_i} + R_\psi(t), \tag{15}$$

where U is the sum of U_{ij} over the nearest neighbors of site i, ζ is a damping coefficient and $R_\phi(t), R_\theta(t)$, and $R_\psi(t)$ are uncorrelated random thermal noise sources. Each of the random variables R has a Gaussian distribution of variance $2k_BT\zeta/\delta t$ where k_B, T, and δt are Boltzmann's constant, the temperature, and the time step, respectively. We measured time in units of β (choosing $\zeta=1$), and used a time step $\delta t=0.0005$. A dynamical equation for $\cos\theta$ rather than θ must be used in order to reach the correct equilibrium states [14]. We verified that our dynamical equations led to the same phase diagram produced by Monte Carlo simulations [12,13].

As in previous numerical studies of defect behavior [15,16], we introduce a disclination line segment counting operator,

$$D^w_{ijkl} \equiv \frac{1}{2}[1 - \mathrm{sgn}\{(\mathbf{w}_i \cdot \mathbf{w}_j)(\mathbf{w}_j \cdot \mathbf{w}_k)(\mathbf{w}_k \cdot \mathbf{w}_l)(\mathbf{w}_l \cdot \mathbf{w}_i)\}], \tag{16}$$

which is unity if a disclination line segment pierces the lattice square defined by the four sites *i*, *j*, *k*, and *l*. We define analogous operators D^u_{ijkl} and D^v_{ijkl} for the **u** and **v** vectors on this lattice square. In principle, either two or none of the three operators should be unity for a given square, and thus we can assign the line segment to one of the classes C_u, C_v, or C_w. In practice, we found a small number of squares

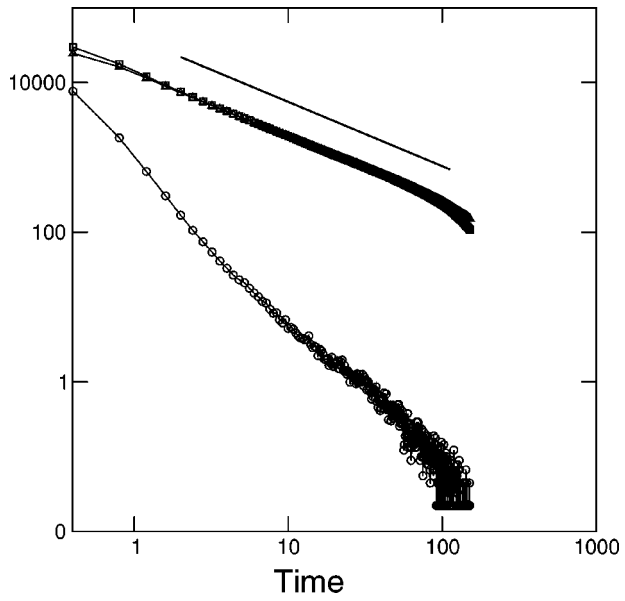

FIG. 2. Log-log plot of the total line length of C_v (○), C_w(□), and C_u(△) class defects for system size 40^3, and parameters $\gamma = 1/2$, $\delta = 4\gamma^2/3 = 1/3$ (corresponding to region B in Fig. 1), as a function of dimensionless time after the quench. The data has been averaged over 60 initial random configurations. The straight line shown at the top of the figure is a power-law fit (offset from the data for the sake of clarity) of the decay with an exponent 0.86.

where only one or all three operators were unity, an artifact of the discreteness of the underlying lattice. We obtained physically reasonable results by classifying the defects on the basis of the operators D^u_{ijkl} and D^w_{ijkl}, assuming that D^v_{ijkl} was unity only if *one* of the two former operators was unity. This procedure always yielded closed defect loops in three dimensions, a reasonable test of our algorithm. We determined the location of the integer-valued defects where either **w** or **u** (or both) rotate by $\pm 360°$ degrees using the algorithm of Ref. [4] which provides an upper bound on these defects. We found very few integer-valued defects using this method, so a more accurate algorithm is not needed.

We quenched the system instantaneously from an initial configuration of random orientations of the three vectors **u**,**v**,**w** (i.e., a high temperature state) to zero temperature (a biaxially ordered state for all $\delta \neq 0$), and then let the system evolve in time according to the dynamical equations (15) monitoring the defect populations both visually and statistically. We studied the model in both two and three dimensions.

In agreement with our arguments above regarding the preferred decay channels, we found three qualitatively distinct types of coarsening behavior depending on the values of γ and δ (we set $\beta = 1$). In regions A and B of Fig. 1 we found a late time coarsening sequence with two defect classes present, consistent with the energy arguments given above. The total line length for each of the three defect classes for system parameters at a point in region B is shown in Fig. 2 for a three-dimensional system and in Fig. 3 for a two-dimensional system. Region B includes the model studied in Ref. [2] (where two defect classes were observed at late

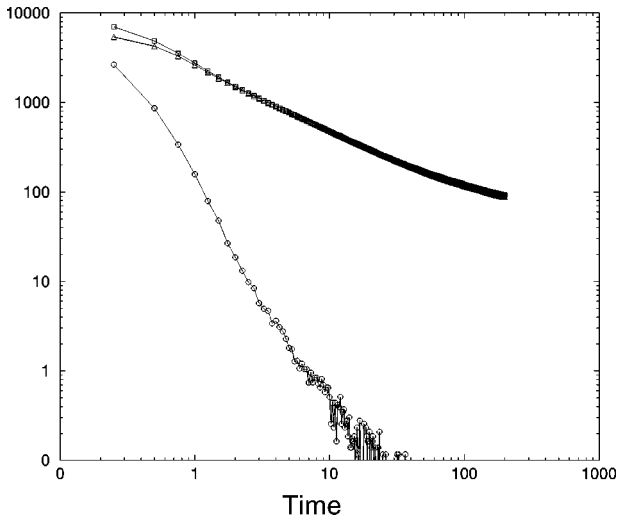

FIG. 3. Log-log plot of the total line length of C_v (○), C_w(□), and C_u(△) class defects for system size 192^2, and parameters $\gamma = 1/2$, $\delta = 4\gamma^2/3 = 1/3$ (corresponding to region B in Fig. 1), as a function of dimensionless time after the quench. The data has been averaged over 80 initial random configurations. Similar behavior is shown in Fig. 22 of Ref. [2].

times), as well as the parametrization of Eq. (2) used in Refs. [12,13], where $\delta = 4\gamma^2/3$ was chosen. In Fig. 4 we show a snapshot of the simulation cell late in the coarsening sequence for the same set of parameters as in Fig. 2. The C_v

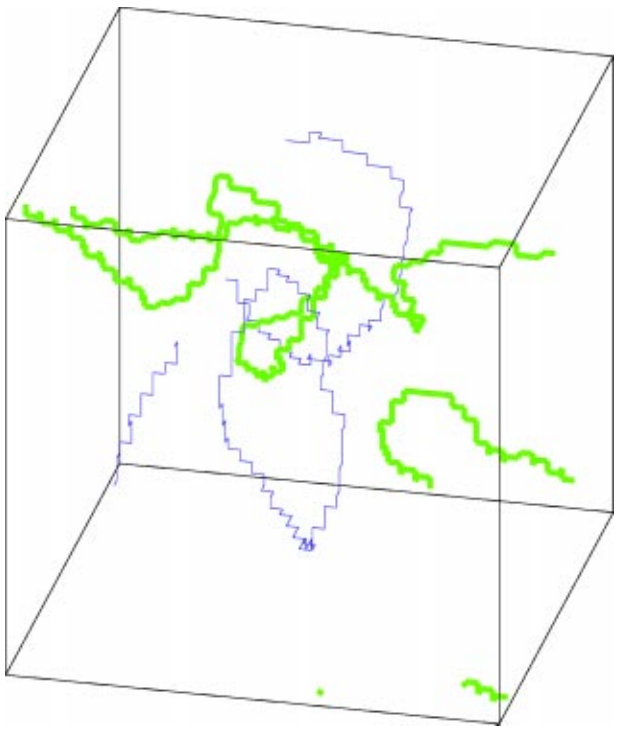

FIG. 4. The configuration of C_u (thin line) and C_w (bold line) class defects for the same system parameters used in Fig. 2, at dimensionless time 80 after the quench. Note that all C_v class defects have vanished at this late time. The C_w and C_u form nonintersecting loops which coarsen independently.

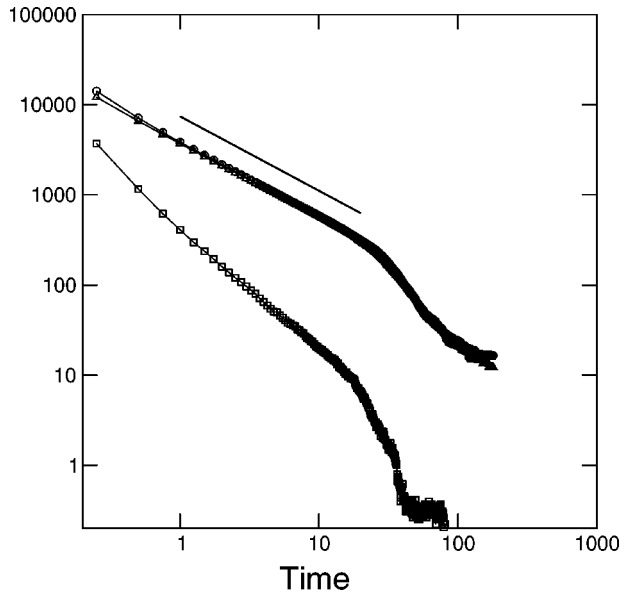

FIG. 5. Log-log plot of the total line length of C_v (○), C_w(□), and C_u(△) class defects for system size 40^3, and parameters $\gamma=0$, $\delta=3.5$ (corresponding to region C in Fig. 1), as a function of dimensionless time after the quench. The data has been averaged over 80 initial random configurations. The straight line shown at the top of the figure is a power-law fit (offset from the data for the sake of clarity) of the decay with an exponent 0.83.

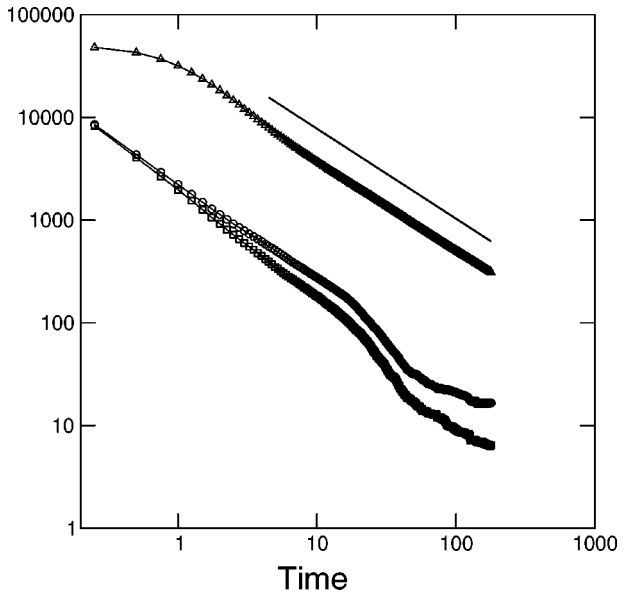

FIG. 6. Log-log plot of the total line length of C_v (○), C_w(□), and C_u(△) class defects for system size 40^3, and parameters $\gamma=1.3$, $\delta=2.8$ (corresponding to region *D* in Fig. 1, near the intersection with regions *C* and *B*), as a function of dimensionless time after the quench. The data has been averaged over 80 initial random configurations. The straight line shown at the top of the figure is a power-law fit (offset from the data for the sake of clarity) of the decay with an exponent 1.01.

class defects have disappeared and the C_u and C_w class defects remain as nonintersecting closed loops. The behavior in region *A* is qualitatively similar with the interchange of C_u and C_v defects. The coarsening behavior in region *C* is qualitatively similar to that observed in regions *A* and *B*, except now the surviving defects are those in classes C_u and C_v. The total line length for each of the defect classes for a system in region *C* is shown in Fig. 5.

For all parametrizations simulated where coarsening at late times involved two classes of defects we never saw apparent line crossings, entanglements, or junction points (the latter obviously would require three classes of defects). The two classes of loops appear to coarsen independently, as can be seen in the animations on our web site [17].

A coarsening sequence with late time survival of only one class of defects appears, as expected from our energy arguments, in region *D*, near any of the vertices. For example, with $\gamma=0.3$, $\delta=2.8$, (near the vertex where regions *B*, *C*, and *D* meet) we find total line lengths as shown in Fig. 6. The C_u defects survive at late times, consistent with our arguments above.

The most interesting and novel coarsening sequence occurs when $\gamma=0$ and $\delta=1$. For these parameters Eq. (8) implies that all three elastic constants are equal, and we found a coarsening sequence with nearly equal populations of the three defects, as shown in Figs. 7 and 8 for a two-dimensional and a three-dimensional system, respectively. This behavior persists over a range of parameters $\delta\sim1.0\pm0.5$ and $\gamma\sim0.0\pm0.2$. Beyond this range the three decay channels, Eqs. (9)–(11), have sufficiently different gains in free energy, Eqs. (12)–(14), such that one or two defect

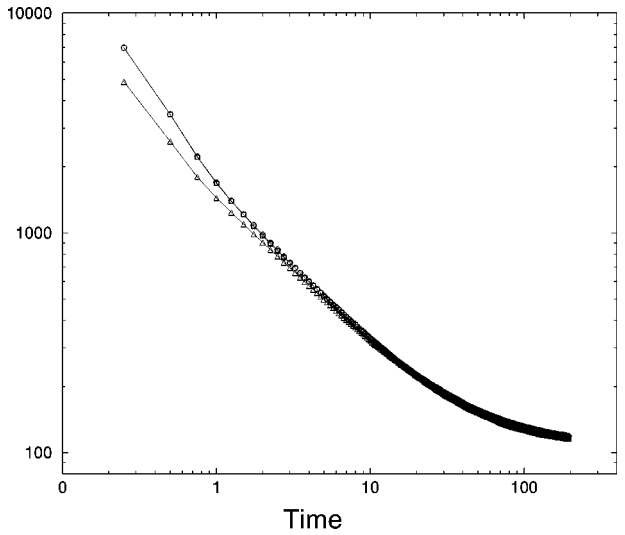

FIG. 7. Log-log plot of the total line length of C_v (○), C_w (□), and C_u (△) class defects for system size 256^2, with parameters $\gamma=0$, $\delta=1$ (where all three elastic constants are equal), as a function of dimensionless time after the quench. The data has been averaged over 60 initial random configurations. While, in principle, the population of the three classes of defects should be equal immediately after the quench, there is a small difference in these populations due to the numerical issues discussed in the text following Eq. (16). Note, however, that the data points for the C_v (○) and C_w (□) classes do overlap.

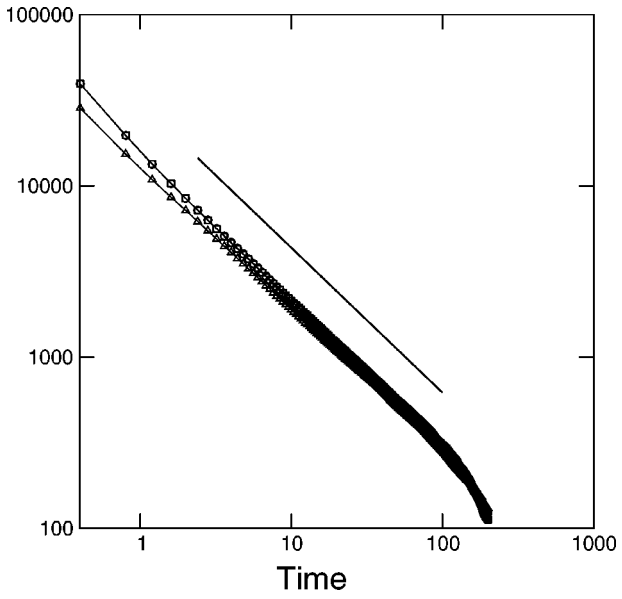

FIG. 8. Log-log plot of the total line length of C_v (○), C_w (□), and C_u (△) class defects for system size 60^3, and parameters $\gamma=0$, $\delta=1$ (where all three elastic constants are equal), as a function of dimensionless time after the quench. The data has been averaged over 40 initial random configurations. The straight line shown at the top of the figure is a power-law fit of the decay with an exponent 0.85. While, in principle, the population of the three classes of defects should be equal immediately after the quench, there is a small difference in these populations due to the numerical issues discussed in the text following Eq. (16). Note, however, that the data points for the C_v (○) and C_w (□) classes do overlap.

classes (depending on the values of γ and δ) dominate at late times. The coarsening sequence for the range of parameters where the three defect classes are present in nearly equal numbers is particularly interesting in three dimensions. We do not find independent loops for each of the defect classes. Rather, soon after the quench a uniform network of junction points where three disclination lines (one from each of the three half-integer classes) meet is formed. These junction points are illustrated in Fig. 9 at late times after the quench. The junction points are distributed in a nearly uniform fashion throughout the simulation cell, and the distance between neighboring points grows on average with time [17]. When the distance between neighboring junction points becomes comparable with the size of the simulation cell (see Fig. 9), the coarsening process is impeded. The final annihilation of the disclination lines can only occur via the shrinkage of individual loops. The formation of loops requires that some pairs of neighboring junction points approach each other, shrinking the line joining them while possibly increasing the length of the other two disclination lines attached to the pair of junction points. Ultimately, the pair of junction points meet at a "pinch point," where four disclination line segments corresponding to two defect classes meet. Subsequently the four line segments dissociate into two nonintersecting single class line segments as can be seen in Fig. 10 and in our animations [17]. When this process has occurred a sufficient number of times, individual disclination loops are formed which then shrink independently.

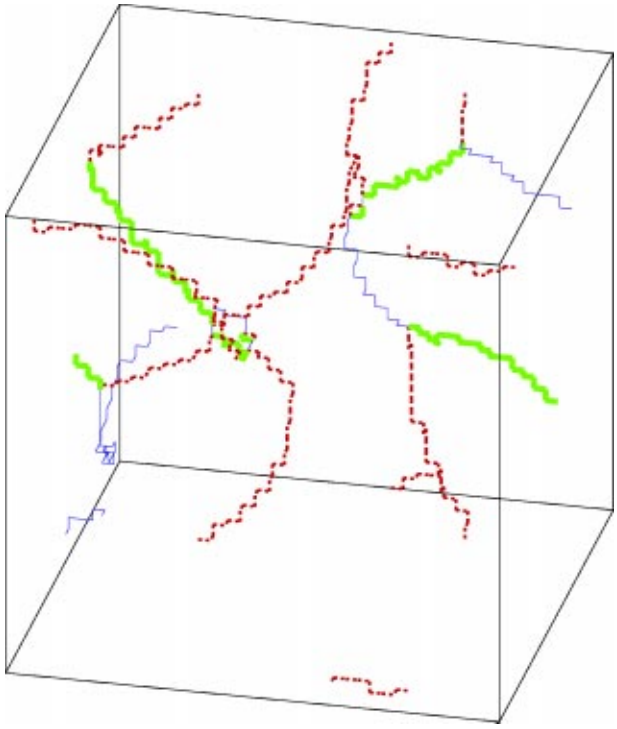

FIG. 9. The configuration of C_u (thin line), C_v (dotted line), and C_w (bold line), class defects for system size 40^3, and parameters $\gamma=0$, $\delta=1$ (where all three elastic constants are equal), at dimensionless time 60 after the quench.

We examined the structure of the junction points, in particular, whether the three disclination line segments meeting at a point are coplanar as one might expect from considerations of force balance. We found most, but not all, of the points have a coplanar geometry. We also examined the nature of the crossover from the region of the parameter space where a network of junction points forms to the regions where only one or two defect classes are present at late times. As γ and (or) or δ are varied away from the point $\gamma=0$, $\delta=1$, we find a network of points where the disclination line segments corresponding to the unfavorable defect class or classes becoming progressively shorter. Finally, as the parameters are varied further, the junction points disappear completely, and independent loops remain.

According to the dynamical scaling hypothesis [18], the total line length of the disclinations in a uniaxial nematic should decay as t^{-1}, though in numerical experiments smaller values of the exponent, of order 0.85–0.90 are typically seen [2]. We have found an exponent of 1.01 when our biaxial system is quenched to a point where only a single class of defect dominates (Fig. 6), and exponents of order 0.85 when the system is quenched to a point where either two or three defect classes dominate at late times (see Figs. 2, 5, and 8). It is interesting to note that even in the case of three defect classes (Fig. 8), there is no significant difference in the exponent, even though the mechanism of coarsening is quite different, as it involves the annihilation of the junction points.

In conclusion, we have shown that the coarsening dynamics of biaxial nematics is very rich, with late time behavior

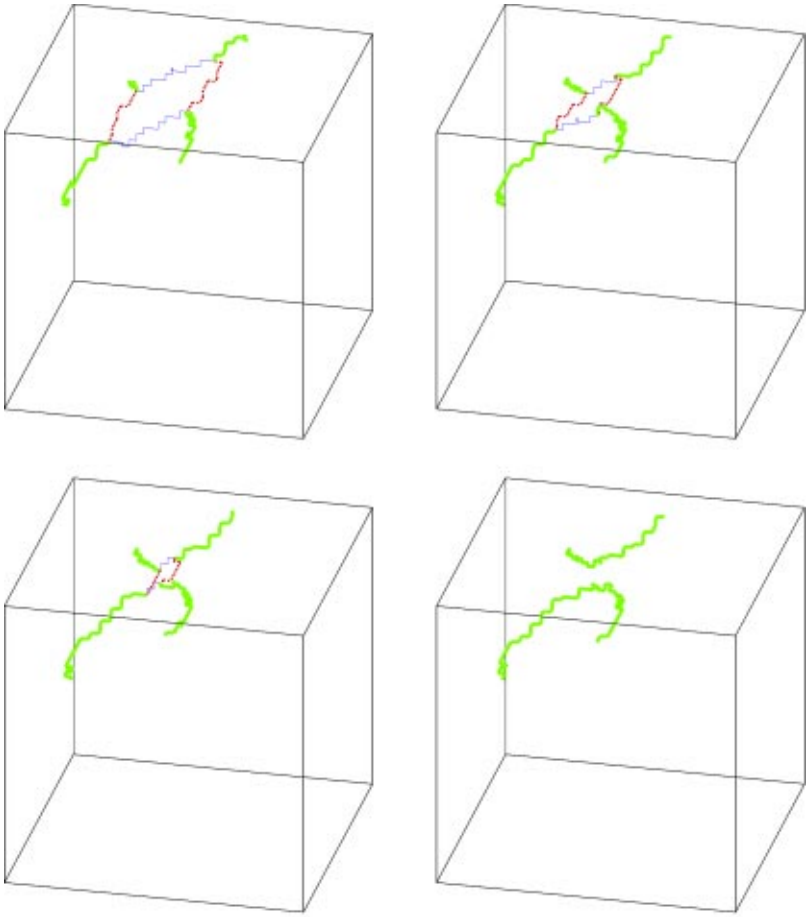

FIG. 10. Snapshots of the simulation cell at four successive dimensionless time steps, $t=85$ (top left), $t=95$ (top right), $t=97$ (bottom left), and $t=100$ (bottom right) with $t=0$ corresponding to the quench. The snapshots illustrate the process by which a pair of junction points annihilate, leaving two independent disclination loops.

governed by either one, two, or three classes of half-integer line defects, depending on the parameters of the system. Simple free energy considerations of the allowed decay channels where defects from two different classes annihilate to form a defect from the third class, allow us to qualitatively predict the relative populations of the defect classes at late times. The predictions of these arguments were confirmed by numerical simulation. Line crossings or entanglements were never observed in the coarsening sequence. When the parameters of the system are such that all three defect classes are present at late times, a network of junction points is formed and a novel coarsening sequence occurs as neighboring points annihilate to allow the creation of independent loops.

We thank S. C. Ying, J. M. Kosterlitz, and M. Zapotocky for helpful discussions, and G. B. Loriot for computational assistance. This work was supported by the National Science Foundation under Grant No. DMR-9873849. Computational work in support of this research was performed at Brown University's Theoretical Physics Computing Facility.

[1] R.E. Blundell and A.J. Bray, Phys. Rev. A **46**, R6154 (1992).
[2] M. Zapotocky, P.M. Goldbart, and N. Goldenfeld, Phys. Rev. E **51**, 1216 (1995).
[3] I. Chuang, B. Yurke, A.N. Pargellis, and N. Turok, Phys. Rev. E **47**, 3343 (1993).
[4] J.L. Billeter, A.M. Smondyrev, G.B. Loriot, and R.A. Pelcovits, Phys. Rev. E **60**, 6831 (1999).
[5] G. Toulouse, J. Phys. (Paris), Colloq. **38**, L67 (1977).
[6] N.D. Mermin, Rev. Mod. Phys. **51**, 591 (1979).
[7] T. De'Neve, M. Kleman, and P. Navard, J. Phys. II **2**, 187 (1992).
[8] V. Poenaru and G. Toulouse, J. Phys. (Paris), Colloq. **8**, 887 (1977).
[9] C. Kobdaj and S. Thomas, Nucl. Phys. B **413**, 689 (1994).
[10] S. Sukumaran and G.S. Ranganath, J. Phys. II **7**, 583 (1997).
[11] J.P. Straley, Phys. Rev. A **10**, 1881 (1974).
[12] G.R. Luckhurst and S. Romano, Mol. Phys. **40**, 129 (1980).
[13] F. Biscarini, C. Chiccoli, P. Pasini, F. Semeria, and C. Zannoni, Phys. Rev. Lett. **75**, 1803 (1995).
[14] C. Goze, V. Ricardo Paredes, R. Carlos Vasquez, D. Ernesto Medina, and A. Hasmy, Phys. Rev. E **63**, 042701 (2001).
[15] P.E. Lammert, D.S. Rokhsar, and J. Toner, Phys. Rev. E **52**, 1778 (1995).
[16] N.V. Priezjev and R.A. Pelcovits, Phys. Rev. E **64**, 031710 (2001).
[17] http://www.physics.brown.edu/Users/faculty/pelcovits/biaxial/
[18] See, e.g., A.J. Bray, Physica A **194**, 41 (1993).